A GENUINELY MULTIDISCIPLINARY JOURNAL

CHEMPLUSCHEM

CENTERING ON CHEMISTRY

Accepted Article

Title: Bimetallic metal organic frameworks: Magnetically separable heterogeneous catalyst for efficient organic transformation and photocatalytic dye degradation

Authors: Jaspreet Kaur Randhawa, Ashish Tiwari, Prateep singh Sagara, and Vicky Varma

A Journal of

ChemPubSoc
Europe

WILEY-VCH   **www.chempluschem.org**

COMMUNICATION

Bimetallic Metal Organic Frameworks as Magnetically Separable Heterogeneous Catalyst for Efficient Organic Transformation and Photocatalytic Dye Degradation

Ashish Tiwari[#][a], Prateep Singh Sagara[#][b], Vicky Varma[b] and Jaspreet Kaur Randhawa*[a]

Abstract: A new bimetallic MOF (BMOF) has been synthesized using iron and zinc as inorganic metal nodes and 1-4, benzenedicarboxylic acid (BDC) as organic linker molecule. BMOF was confirmed with Single crystal X-ray diffraction (SCXRD), X-ray photoelectron spectroscopy (XPS), Transmission electron microscopy-high angle annular dark-field imaging (TEM-HAADF), Field emission scanning electron microscopy-energy dispersive x-ray analysis (FESEM-EDX), Vibrating sample magnetometer (VSM) and inductively coupled plasma-mass spectrometry (ICP-MS) analysis. The synthesized BMOF shows excellent optical and magnetic properties. BMOF acts as a heterogeneous catalyst and show high catalytic activity towards bis(indolyl)methane synthesis and photocatalytic degradation of methylene blue (MB) under visible light illumination.

The motive of crystal engineering is to develop new crystals with precise control of morphology, porosity and functionality.[1] Metal organic frameworks (MOFs) are one such a class of cross breed products of crystal engineering, comprising nodes of transition metals (M^{2+}, M^{3+} and M^{4+}) connected by organic linkers of amine and carboxylate functionalities that unlock the potential for new crystal design for respective applications.[2] The node and linker union form assemblies from linear, angular, trigonal or tetrahedral symmetries with variety of frameworks and surface properties.[3] For example, divalent M^{2+} metal nodes form fragile framework [4] act as week Lewis acid sites that limit their catalytic activity. Similarly, tetravalent metal cations (M^{4+}) provide stronger Lewis acid sites [5], but the synthetic route for obtaining phase pure crystals of these metal nodes are yet to be developed.

Designing bimetallic MOF[6],[7] containing more than one metal nodes could be one of the alternatives for achieving improved properties as compared to their monometallic counterparts.[8] For instance, MOF-5 is moisture sensitive under atmospheric conditions and doping Ni(II) in MOF-5 enhance its hydrostability.[9] Likewise, bimetallic Zn-Cu BTC MOF revealed higher desulfurization capacity than the monometallic Cu-BTC and even zeolites.[10] Similar studies showed that bimetallic MOF have superior catalytic activities over monometallic MOF being used as heterogeneous catalyst for organic coupling reactions[11],[12] such as heck reaction,[13] C-H bond halogenation,[14] catalyzing OER reactions,[15] selective oxidation of aromatic substrates[16], Knoevenagel condensation[17] and Suzuki coupling reaction.[18],[19]

[a]   Mr. Ashish Tiwari and Dr. Jaspreet Kaur Randhawa*
       School of Engineering, Indian Institute of Technology Mandi,
       Mandi, Himachal Pradesh, India, 175005.
       E-mail: jaspreet@iitmandi.ac.in
[b]   Mr. Prateep Singh Sagara and Mr. Vicky Varma
       School of Basic Sciences, Indian Institute of Technology Mandi,
       Mandi, Himachal Pradesh, India, 175005.
[#]   These authors contributed equally to this work.

Supporting information for this article is given via a link at the end of the document.

Besides, some studies have dealt with photocatalytic properties of hybrid MOFs such as Fe/M(M=Mn, Co, Ni) MOFs, Fe(II)@MIL-100(Fe) and MIL-53(Fe) MOFs.[20],[21] Thus, the rational design and synthesis of hybrid structure with multi-functionalities could achieve enhanced physicochemical properties and efficiency.

Inspired with the possibility to improve the properties through introducing a new metal component in MOF, we hereby report the synthesis and crystal structure of a new bimetallic MOF composed of divalent Zn and trivalent Fe ions linked with 1, 4-benzenedicarboxylic (BDC) acid to form Fe-Zn BDC MOF.

The pristine MOF doped or incorporated with another metal provide a scope to tune the electronic band gap. Recent studies show that the incorporation of iron as second metal in MOF decreases the band gap of parent MOF and enhanced its absorption into visible region.[22] The band gap values of MIL-53 and MOF-5 are 2.6 eV[23] and 3.5 eV[24] whereas the BMOF in present work assessed band gap value ca. 1.9 eV which suggest that the presence of second metal decrease the band gap. As, Fe-Zn BDC BMOF exhibits the band gap of 1.90 eV and this was exploited for the photocatalytic degradation of methylene blue (MB). The photocatalytic degradation efficiency ca. 57% was achieved in 90 minutes under visible light illumination. Organic transformation of indoles to bis(indolyl) is one of the most ubiquitous heterocycle among natural products. This encompass wide applications i.e. antibacterial, antifungal, antimicrobial, anti-inflammatory and anticancer activities.[25] Variety of Lewis acid catalysts such as metal halides, nitrates, and oxychlorides were employed in this reaction with harsh reaction conditions and solvents.[26] The present work demonstrates use of Fe-Zn BDC BMOF as heterogeneous catalysts for the synthesis of bis(indolyl)methanes. The reaction shows 94% conversion efficiency of bis(indolyl)methanes. The catalyst can be efficiently recovered from the reaction mixture magnetically and reused further for catalytic activity. BMOF was obtained from a single step solvothermal synthesis method using $Zn(NO_3)_2.6H_2O$ and $Fe(NO_3)_3.9H_2O$ in DMF/ethanol solvent in 4:1 ratio. The metal salts were thoroughly mixed with 1, 4-benzenedicarboxylic (BDC) acid by magnetic stirring for 30 min. This solution was then transferred to a Teflon-lined stainless-steel Parr autoclave and heated to 150°C for 20 hrs. A pale yellow colored crystals, stable in atmospheric conditions were attained. Single crystal X-ray diffraction analysis revealed the formation of monoclinic crystal system with C_2/C space group having 3D porous framework. The asymmetric unit as shown in Figure 1b reveals that each Zn(II) is forming coordinate bonds with a slightly distorted geometry with three oxygen atoms (O_1, O_2, O_5) from three different BDC ligands. The fourth coordination is satisfied by carboxylate oxygen (O_3) of another BDC linker (Figure 1a). The second metal Fe(III) is surrounded by six oxygen atoms. The Zn-O bond distance are in the range of 1.944-1.978 Å and Fe-O bond lengths are in range of 2.042 to 2.213 Å.

COMMUNICATION

The carboxylate linker offers the conformational freedom where it bridges with metal node in three different modes that includes monodentate (κ_1), monoatomic bridging (μ_2-κ_2) and bidentate bridging (μ_2-κ_1:κ_1) as shown in Figure 1e.[27] The distance calculated between Zn-Zn, Fe-Zn and Fe-Fe are 6.5098, 3.2549 and 14.59 Å respectively. The SCXRD studies revealed that half of the three BDC molecules links with one Zn(II) ion and half of two BDC molecules link with Fe(III) ion. Fe-Zn BDC BMOF crystal forms pillared square grid framework (Figure 1d) where the complete polymorphic unit arrangement underlines Zn atom coordinated to four oxygen atoms in tetrahedral symmetry and Fe atom is coordinated with 6 oxygen atom in octahedral symmetry respectively. In a larger preview, intra-framework space is formed of 2D layers connected together by the ligand to generate 3D structure. The complete crystal structure along b axis, space fill diagram and polyhedron structure of unit cell are shown in Figure 1d, Figure S0 and S0a (SI) respectively.

The bulk identity of Fe-Zn BDC BMOF crystals was studied by comparing the PXRD pattern of the as synthesized sample with the simulated pattern as shown in Figure 2a without any pre-treatment. The similarity of the patterns indicates that crystals are formed in pure phase. XPS analysis illustrates distinct characteristic peaks of C1s, O1s, Fe2p and Zn2p in full survey spectrum of Fe-Zn BDC BMOF (Figure 2b). Further, deconvoluted Fe2p spectra showed two distinct peaks at binding energies of 711.7 eV for Fe2p$_{3/2}$ and 719.2 eV for Fe2p$_{1/2}$ respectively, accompanied by one prominent shake-up satellite peak (714 eV) which are characteristic peaks of Fe^{3+} (Figure S1 SI).[28] Additionally, deconvoluted Zn2p spectra showed two distinct peaks at binding energies of 1021.5 eV for Zn2p$_{3/2}$ and 1044.6 eV for Zn2p$_{1/2}$ demonstrating the presence of Zn^{2+} (Figure S2 SI).[29] The deconvolution of O1s and C1s also displayed various species of hydroxyl and carboxyl groups as shown in Figure S3 and S4 (SI).[30] Optical properties as studied by diffuse reflectance (DRS) spectra showed absorption peaks at wavelength of 330 nm (Figure S5 SI). The band gap value assessed from the steep absorption edges was calculated to be 1.9 eV (Figure 2c) using Kubelka–Munk (K-M) function as described in experimental section.[31] This band gap specified visible light absorption of Fe-Zn BDC BMOF. Figure 2d shows magnetic hysteresis (M-H) curve recorded at 300K. Fe-Zn-BDC BMOF showed saturation magnetization (M$_s$) of 11.92 emu/gm. FC and ZFC curves studied at 500 Oe (Figure S6 SI) also stand with the strong magnetic behavior. Magnetic properties are advantageous for separation of catalyst after heterogeneous catalysis. Hence, magnetic behavior was perceived using a magnet in the aqueous suspension of Fe-Zn BDC when taken near to magnet, corresponding aggregation towards magnet was clearly observed (Figure S21 SI). This observation confers easy separation and reusability of catalyst after catalytic reactions. FESEM images of Fe-Zn BDC BMOF revealed the formation of micron sized crystals with rod like morphology as shown in Figure S7 (SI). Elemental analysis using FESEM-EDX confirmed the presence of Fe and Zn as shown in Figure S8 (SI). TEM image of grinded sample as displayed in Figure S9 (SI) revealed the presence of small agglomerates with an average size of ca 20 nm. High-angle annular dark-field scanning transmission electron microscopy (HAADF-STEM) mapping confirmed the presence of Fe and Zn uniformly distributed throughout the sample, as shown in Figure S10 (SI). The inductively coupled plasma atomic emission spectroscopy

(ICP-MS) data (Table S1 SI) revealed the presence of iron and zinc in Fe-Zn BDC BMOF with slightly less Zn^{2+} content than Fe^{3+}. Fe-Zn-BDC BMOF has a zeta potential value of −3.54 mV. The particle size of grinded Fe-Zn-BDC BMOF revealed from TEM images as well as measured average hydrodynamic size from DLS was in the range of 10–100 nm which favor the negative zeta potential value.

Thermogravimetric experiments were undertaken to analyse the thermal stability as depicted in Figure S11 (SI). The thermogram demonstrates steady weight loss from room temperature to 350°C which constitute to removal of solvents. Above 350°C, the decomposition of BDC linker from the framework take place with complete breakdown of the structure at around 500°C. FTIR spectra as shown in Figure S12 (SI) highlights the characteristic bridging modes of metal oxygen bonds and functional groups. Fe-Zn BDC BMOF shows characteristic bands of BDC at 1371 and 1565 cm^{-1} for symmetric and asymmetric stretching vibrations. The separation of 194 cm^{-1} between antisymmetric and symmetric bridging carboxyl groups is similarly reported.[32] The peaks in the range of 1602–1560 cm^{-1} and 1406–1364 cm^{-1} may be attributed to bridging and chelating carboxyl groups.[32] The metal oxygen bonds were identified at 560 cm^{-1} which correspond to Fe-O and at 420 cm^{-1} for Zn-O respectively. A broad peak ranging 3000-3400 cm^{-1} corresponds to O-H stretching of carboxylic groups and surface adsorbed hydroxyl groups.[33] Raman spectra as depicted in Figure S13 (SI) displayed various bands spotted for Fe and Zn based MOF. The bands spotted at 635, 864, 1139, 1433, and 1615 cm^{-1} resemble for MOF-5 respectively.[34] Further, the present BMOF shows specific Fe-MIL MOF bands in its spectrum featuring at 210 and 450 to 600 cm^{-1} which may be attributed to crystalline iron based framework structure and lattice vibrations with network binding modes respectively.[35] The band spotted at 1617 cm^{-1} could be assigned to C=C stretching mode of BDC only appears due to g parity under C$_i$ symmetry. Additionally, bands at 1535 and 1430 cm^{-1} may be attributed to in-plane asymmetric and symmetric stretching of v$_{asym}$ (COO) and v$_{sym}$ (COO) respectively.[33] Optical behavior of BMOF was analyzed using photoluminescence (PL) spectroscopy under experimental conditions with excitation wavelength of 280 nm. Figure S14 (SI) shows two distinct emission peaks at 445 and 485 nm and one small shoulder peak at 418 nm. The peaks observed in between 410-430 nm corresponds to Fe (III) and peak at 485 nm corresponds to Zn (II) luminescence peak. The emission at 445 nm is due to intra-ligand emission. However, emission bands of the carboxylate ligands originated from π*→n transition are weak and it is considered that carboxylate ligands have no significant contribution to the fluorescent emission of coordinated structures.[36] Specific surface area and porous structures were determined by nitrogen adsorption and desorption isotherms at low relative pressure and the data is presented in Figure S15 and S16 (SI). A sequential increase in the adsorption isotherms from low to high relative pressure strongly relates significant interactions of guest molecules with adsorbents. BET surface area, pore volume and average pore width were calculated to be 107.6 m^2/g, 0.133 cc/g and 16.87 Å respectively. High surface area contributes towards high catalytic activity by increasing adsorption of organic molecules from aqueous solutions on the surface of photocatalyst. Inspired by the band gap value of 1.9 eV of Fe-Zn BDC MOF, photocatalytic degradation of MB in aqueous solution under

COMMUNICATION

visible light was undertaken as illustrated in Figure 3. The absorption maximum of MB at 664 nm decreased with time under the irradiation of the visible light, suggesting the degradation of MB. Control experiments were executed to compare the degradation efficiencies of MB in three different environments viz., in dark condition, with H_2O_2 alone and in presence of Fe-Zn BDC alone respectively. Photocatalytic activity was found to be concentration dependent as evident from Figure 3, ca. 57% of MB was photo catalytically degraded after 90 min of visible light illumination using 10 mg/L of photocatalyst concentration. However, in dark conditions and in presence of H_2O_2 alone no obvious degradation of MB was observed. The visible light photocatalytic activity enhanced significantly by the addition of H_2O_2. This is because, H_2O_2 effectively act as charge carrier scavenger which reduces the possibility of the recombination of photo-generated charge carriers and accelerate the generation of hydroxide radicals. The generated hydroxide radical species rapidly degrade MB and enhance the photocatalytic activity.[28] For the purpose of practical application it is essential to evaluate the long term stability of the photocatalyst. Thus, the reusability studies were carried out for five times and similar degradation rate 53% degradation was achieved. The chemical stability of photocatalyst was also evaluated after the degradation reaction and comparison of PXRD spectra (Figure S22 SI) before and after photocatalysis show the structural integrity of BMOF.

Photocatalytic degradation mechanism of MB could be deliberated based on semiconductor band gap theory.[38] A detailed mechanism is presented in Figure S18 (SI). Under visible light illumination, when a photon having energy equal to or greater than the band gap of photocatalyst falls on the sample, excitation of electrons from valence band to conduction band happens with the formation of holes in the valence band. The generated holes in valance band immediately oxidize the surface adsorbed dye molecules or produce hydroxyl radicals (•OH) on reacting with surface adsorbed hydroxyl ions (OH^-) due to strong oxidizing nature. Band gap energy (ca. 1.9 eV) signify that produced holes possess high oxidation potential for dye degradation. In addition, hydroxyl radicals also contribute in oxidizing surface adsorbed dye molecules to accelerate the photodegradation. In the meantime, electrons present in the conduction band react with the surface adsorbed molecular oxygen (O_2) to produce superoxide radicals (O_2^-). Strong oxidant capability of generated superoxide radicals leads to degradation of MB. At the same time, electrons in conduction bands activate H_2O_2 and generate hydroxyl radicals which significantly degrade MB.[39] The photocatalyst exhibits good magnetic and photodegradation properties making them advantageous for degradation of organic pollutants in waste water treatment.

Further, Fe-Zn BDC BMOF was employed for organic coupling reactions of indoles and benzaldehydes at 80°C in 1, 2 dichloroethane (DCE) solvent as summarized in Scheme 1 and Table S2 (SI), the product yield was quiet significant. The effect of different solvents on the product yield of bis(indolyl)methane was also examined as shown in the Table S3 (SI). For solvent screening, the reaction was performed using Indole and benzaldehyde (1:2) with catalyst (10 mg) at 80°C for 12 hours in different solvents. When nonpolar solvents such as 1, 2 dichloroethane and tetrahydrofuran were used for the bis(indolyl)methane synthesis, the product yield was found 94 and 60% respectively. When polar solvents such as N, N-

dimethylformamide (DMF), dimethyl sulfoxide (DMSO), acetonitrile, methanol and water were used; the product yields were ca. 75, 86, 81, 80 and 50% respectively. Further, on the basis of high product yield achieved for bis(indolyl)methane synthesis in 1, 2 dichloroethane, a number of various aromatic groups substituted aldehydes were reacted with indoles to produce bis(indolyl)methanes compounds (Table 1 (1-12)). We have screened a series of aromatic compounds containing electron donating and electron withdrawing groups and heteroaromatic compounds which underwent to reaction with indole easily to afford a wide range of substituted bis(indolyl)methanes with high product yield. Aromatic aldehydes having electron withdrawing groups (i.e. NO_2, CN, and F) react faster than the simple benzaldehyde while electron donating groups (i.e. CH_3, OH) which deactivated aryl aldehydes leading to slow down the reaction resulting delay in product formation. On the other side, the heteroaromatic aldehydes such as furfural and 2-thiophene carboxaldehyde were more reactive (Entry 8 and 9, Table 1). A detailed product yield for synthesized substituted bis(indolyl)methanes is tabulated in Table 1 appropriately. A plausible mechanism for the synthesis of the bis(indolyl)methane is shown in Figure S19 (SI). The proposed mechanism for organic transformation illustrates that carbonyl group in the aromatic aldehyde is activated by Fe-Zn BDC followed by the nucleophilic addition of the indole which yields intermediate 1, a transformation from intermediate 1 to intermediate 2 takes place by elimination of water molecule. Further, nucleophilic addition of another indole molecule on intermediate 2 gives intermediate 3 followed by aromatization to get the desired product bis(indolyl)methane. The synthesis of bis(indolyl)methane was determined superior using Fe-Zn BDC in terms of product yield 94% as compared to other catalysts such as metal halides and nitrates. A detailed comparison[40] of various catalysts used for bis(indolyl) methane synthesis is summarized in Table S4 (SI). In addition, the reusability of the catalyst was also examined and no significant change in catalytic activity was found even after seven cycles of reaction (Figure S20 SI). The results in the present work show that using Fe-Zn BDC, a series of bis(indolyl)methane compounds can be synthesized with high product yields being an alternative to metal halides and nitrates catalysts.

In summary, a new bimetallic metal organic framework (BMOF) has been synthesized using Fe and Zn as metal nodes with 1, 4-benzenedicarboxylic acid as linker molecule named as Fe-Zn BDC BMOF. The synthesized Fe-Zn BDC BMOF showed superior catalytic activity in organic transformation of indoles and aromatic benzaldehydes into bis(indolyl)methane with high product yield of ca. 94%. In addition, photocatalytic degradation of methylene blue with efficiency of ca. 57% in 90 minutes under visible light irradiation was also achieved. With the development of preparation and characterization procedure a well-defined bimetallic MOF can be obtained. The design of bimetallic MOF in terms of additional properties and versatility might be anticipated in various course of applications.
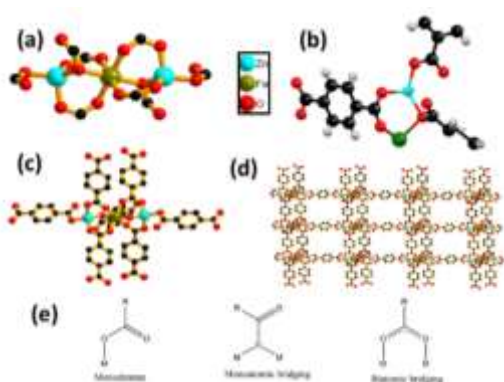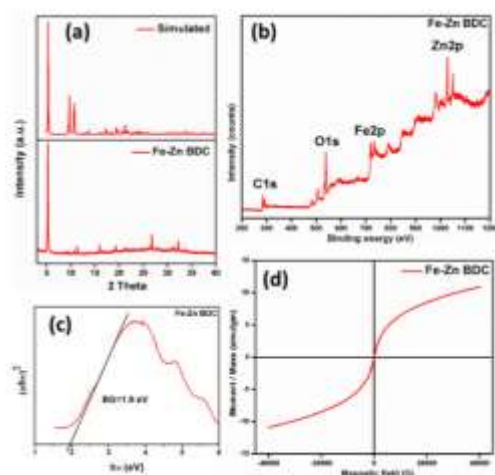
COMMUNICATION

Figure 1. SCXRD analysis of Fe-Zn BDC crystals (a) metal coordinated polyhedron, (b) asymmetric unit of a crystal, (c) a unit cell structure, (d) crystal structure along b axis and (e) binding moods of metals with BDC linker. (Colour code: Fe-green, Zn-sky blue, O-Red and C-Black respectively).
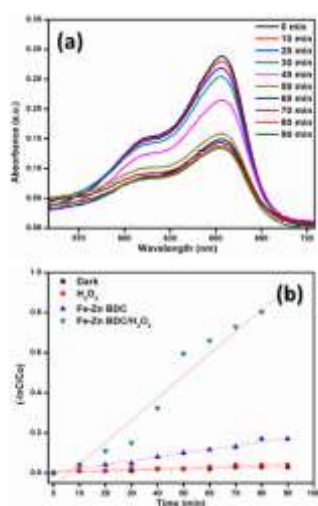
Figure 3. (a) Sequential time dependent photodegradation of MB using Fe-Zn BDC, (b) $-\ln(C/C_0)$ vs. time curve for photodegradation of MB along with control experiments. Experimental conditions: MB concentration (10^{-5} mol/L), 10 µL of 30% H_2O_2 and photocatalyst concentration (10 mg).

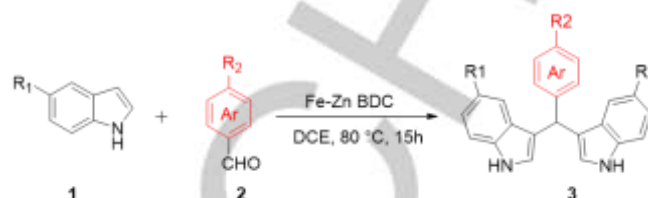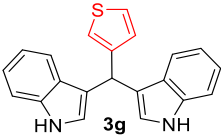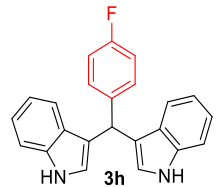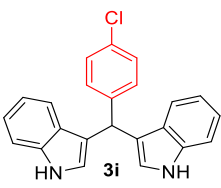**Scheme 1.** Synthesis of bis(indolyl)methanes.
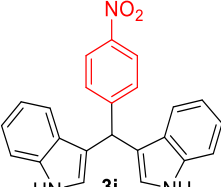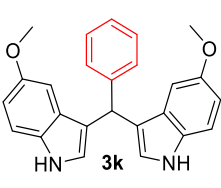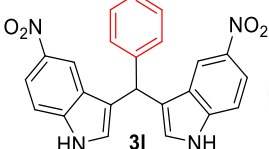
Table 1. Substrates scope for the formation of substituted bis(indolyl)methanes.

Figure 2. (a) PXRD and simulated XRD spectra, (b) XPS full survey spectra, (c) DRS plots for band gap assessment and (d) Hysteresis (M-H) curve of Fe-Zn BDC BMOF.

Entry[a]	Product code	Product [3 a-l]	Time [h]	Yield[b] [%]
1	a	3a	12	94
2	b	3b	14	89
3	c	3c	14	90
4	d	3d	13	93
5	e	3e	10	97
6	f	3f	15	89

For internal use, please do not delete. Submitted_Manuscript

COMMUNICATION

7	g	**3g** (thiophen-3-yl substituted bis(indolyl)methane)	13	85
8	h	**3h** (4-fluorophenyl substituted bis(indolyl)methane)	13	91
9	i	**3i** (4-chlorophenyl substituted bis(indolyl)methane)	13	90
10	j	**3j** (4-nitrophenyl substituted bis(indolyl)methane)	10	95
11	k	**3k** (phenyl substituted bis(5-methoxyindolyl)methane)	11	90
12	l	**3l** (phenyl substituted bis(5-nitroindolyl)methane)	12	91

[a]Indole [2.0 mmol], aldehyde [1.0 mmol], catalyst amount [10 mg] and 1, 2 dichloroethane (DCE) [3.0 mL]. [b]Isolated yields.

Supplementary Information

Material synthesis, characterisation and single crystal data are detailed in supplementary information. X-ray structure: CCDC 123456 (1) is via Cambridge crystallographic data centre.

Acknowledgements

Conflict of interest

The authors declare no conflict of interest.

References

[1] N. Stock, S. Biswas, *Chem. Rev.* **2012**, *112*, 933–969.
[2] H.-C. Zhou, S. Kitagawa, *Chem. Soc. Rev.* **2014**, *43*, 5415–5418.
[3] M. Eddaoudi, D. F. Sava, J. F. Eubank, K. Adil, V. Guillerm, *Chem. Soc. Rev.* **2015**, *44*, 228–249.
[4] T. Devic, C. Serre, *Chem. Soc. Rev.* **2014**, *43*, 6097–6115.
[5] S. Furukawa, J. Reboul, S. Diring, K. Sumida, S. Kitagawa, *Chem. Soc. Rev.* **2014**, *43*, 5700–5734.
[6] D. Zhao, X. H. Liu, J. H. Guo, H. J. Xu, Y. Zhao, Y. Lu, W. Y. Sun, *Inorg. Chem.* **2018**, *57*, 2695–2704.
[7] P. P. Cui, X. Du Zhang, P. Wang, Y. Zhao, M. Azam, S. I. Al-Resayes, W. Y. Sun, *Inorg. Chem.* **2017**, *56*, 14157–14163.
[8] D. S. Sholl, R. P. Lively, *J. Phys. Chem. Lett.* **2015**, *6*, 3437–3444.
[9] H. Li, W. Shi, K. Zhao, H. Li, Y. Bing, P. Cheng, *Inorg. Chem.* **2012**, *51*, 9200–9207.
[10] T. Wang, X. Li, W. Dai, Y. Fang, H. Huang, *J. Mater. Chem. A* **2015**, *3*, 21044–21050.
[11] Y.-S. Kang, Y. Lu, K. Chen, Y. Zhao, P. Wang, W.-Y. Sun, *Coord. Chem. Rev.* **2019**, *378*, 262–280.
[12] D. Zhao, X.-H. Liu, C. Zhu, Y.-S. Kang, P. Wang, Z. Shi, Y. Lu, W.-Y. Sun, *ChemCatChem* **2017**, *9*, 4598–4606.
[13] A. Zhou, R. M. Guo, J. Zhou, Y. Dou, Y. Chen, J. R. Li, *ACS Sustain. Chem. Eng.* **2018**, *6*, 2103–2111.
[14] X. L. Lv, K. Wang, B. Wang, J. Su, X. Zou, Y. Xie, J. R. Li, H. C. Zhou, *J. Am. Chem. Soc.* **2017**, *139*, 211–217.
[15] J. Zhou, Y. Dou, A. Zhou, L. Shu, Y. Chen, J. R. Li, *ACS Energy Lett.* **2018**, *3*, 1655–1661.
[16] A. W. Stubbs, L. Braglia, E. Borfecchia, R. J. Meyer, Y. Román-Leshkov, C. Lamberti, M. Dincǎ, ACS Catal. 2018, 8, 596–601.
[17] A. Dhakshinamoorthy, N. Heidenreich, D. Lenzen, N. Stock, *CrystEngComm* **2017**, *19*, 4187–4193.
[18] A. Dhakshinamoorthy, H. Garcia, *Chem. Soc. Rev.* **2014**, *43*, 5750–5765.
[19] J. Huang, W. Wang, H. Li, *ACS Catal.* **2013**, *3*, 1526–1536.
[20] C.-C. Wang, J.-R. Li, X.-L. Lv, Y.-Q. Zhang, G. Guo, *Energy Environ. Sci.* **2014**, *7*, 2831–2867.
[21] Q. Sun, M. Liu, K. Li, Y. Han, Y. Zuo, F. Chai, C. Song, G. Zhang, X. Guo, *Inorg. Chem. Front.* **2017**, *4*, 144–153.
[22] N. A. Surib, L. C. Sim, K. H. Leong, A. Kuila, P. Saravanan, K. M. Lo, S. Ibrahim, D. Bahnemann, M. Jang, *RSC Adv.* **2017**, *7*, 51272–51280.
[23] R. Panda, S. Rahut, J. K. Basu, *RSC Adv.* **2016**, *6*, 80981–80985.
[24] J. Gascon, M. D. Hernández-Alonso, A. R. Almeida, G. P. M. van Klink, F. Kapteijn, G. Mul, *ChemSusChem* **2008**, *1*, 981–983.
[25] A. Andreani, S. Burnelli, M. Granaiola, A. Leoni, A. Locatelli, R. Morigi, M. Rambaldi, L. Varoli, L. Landi, C. Prata, M. V. Berridge, C. Grasso, H. H. Fiebig, A.M. Burger, M. W. Kunkel, *J. Med. Chem.* **2008**, *51*, 4563–70.
[26] M. Shiri, M. A. Zolfigol, H. G. Kruger, Z. Tanbakouchian, *Chem. Rev.* **2010**, *110*, 2250–2293.
[27] P. Saxena, N. Thirupathi, *Polyhedron* **2015**, *98*, 238–250.
[28] J. Duan, S. Chen, C. Zhao, *Nat. Commun.* **2017**, *8*, 15341.
[29] S. Gadipelli, Z. Guo, *Chem. Mater.* **2014**, *26*, 6333–6338.
[30] Y. Wu, H. Luo, H. Wang, *RSC Adv.* **2014**, *4*, 40435–40438.
[31] Z. Bin Nie, M. Zhang, T. Su, L. Zhao, Y. Y. Wang, G. Y. Sun, Z. M. Su, *RSC Adv.* **2017**, *7*, 31544–31548.
[32] T. R. Whitfield, X. Wang, L. Liu, A. J. Jacobson, *Solid State Sci.* **2005**, *7*, 1096–1103.
[33] K. Tan, N. Nijem, P. Canepa, Q. Gong, J. Li, T. Thonhauser, Y. J. Chabal, *Chem. Mater.* **2012**, *24*, 3153–3167.
[34] S. Bordiga, C. Lamberti, G. Ricchiardi, L. Regli, F. Bonino, A. Damin, K. P. Lillerud, M. Bjorgen, A. Zecchina, *Chem. Commun.* **2004**, *10*, 2300–2301.
[35] X. Li, L. Lachmanski, S. Safi, S. Sene, C. Serre, J. M. Grenèche, J. Zhang, R. Gref, *Sci. Rep.* **2017**, *7*, 13142-13153.
[36] S. S. Chen, J. Fan, T. A. Okamura, M. S. Chen, Z. Su, W. Y. Sun, N. Ueyama, *Cryst. Growth Des.* **2010**, *10*, 812–822.
[37] E. M. Dias, C. Petit, *J. Mater. Chem. A* **2015**, *3*, 22484–22506.
[38] C. Singh, A. Goyal, S. Singhal, *Nanoscale* **2014**, *6*, 7959–70.
[39] M. Saha, S. Mukherjee, S. Kumar, S. Dey, A. Gayen, *RSC Adv.* **2016**, *6*, 58125–58136.

For internal use, please do not delete. Submitted_Manuscript

COMMUNICATION

[40]   M. Shiri, M. A. Zolfigol, H. G. Kruger, Z. Tanbakouchian, *Chem. Rev.*
         2010, *110*, 2250–2293.

WILEY-VCH

COMMUNICATION

Table of Content

A new bimetallic metal organic framework BMOF (Fe-Zn BDC) is synthesisd using Fe and Zn as metal nodes with 1, 4-benzenedicarboxylic acid as linker molecule. BMOF showed superior catalytic activity in organic transformation of indoles and aromatic benzaldehydes into bis(indolyl)methane with high product yield of ca. 94%. In addition, photocatalytic degradation of methylene blue with efficiency of ca. 57% in 90 minutes under visible light irradiation was also achieved.

For internal use, please do not delete. Submitted_Manuscript